Mining Thermophile Genomes for New PETases with Exceptional Thermostabilities Using Sequence Similarity Networks

Zhenyu Hu, Kody Klupt, David L. Zechel, Zongchao Jia, and Graeme Howe*

Enzymatic hydrolysis of polyethylene terephthalate (PET) is a promising technology for advancing a circular PET economy. Several PET-degrading α/β hydrolases have been identified, but the full potential of this enzyme family to catalyze PET hydrolysis remains largely unexplored. To address this, sequence similarity networks are employed to investigate the α/β hydrolase fold-5 subfamily (IPR029059) for new PETases. Priority is given to sequences from thermophiles, as thermostable enzymes are likely more suitable for industrial applications. Ten enzymes with ≈20% sequence identity to the well-known LCC-PETase are identified, and seven are successfully overexpressed and purified for in vitro characterization. Each enzyme catalyzes the hydrolysis of *p*-nitrophenyl butyrate, a mimic of trimeric PET, and emulsified PET nanoparticles. Notably, three enzymes are also capable of hydrolyzing PET films. Novel PETases exhibit melting temperatures (T_m) exceeding 55 °C and only modest losses of activity after incubation at 70 °C for 24 h. The crystal structure of AroC ($T_m = 85$ °C) is resolved to 2.2 Å, revealing several salt bridges that likely confer thermostability, and a unique loop that is conserved among the PETases described here. These novel enzymes will enable engineering campaigns to generate thermostable and catalytically efficient PETases for use as industrial biocatalysts.

1. Introduction

Polyethylene terephthalate (PET) is a thermoplastic polymer synthesized through the condensation reaction of ethylene glycol (EG) and terephthalic acid (TPA). PET is widely utilized for its exceptional properties including chemical inertness, thermal stability, durability, tensile strength, and light weight. These qualities make it an ideal material for applications in food packaging, medical devices, and electrical equipment.[1] PET production accounts for ≈8% of the world's annual plastic production, but less than 50% of PET waste is currently recycled.[2] The chemical inertness of PET waste renders these materials extremely difficult to degrade, such that these materials represent a severe concern for our environment. Several PET recycling methods have been established, including mechanical, chemical, and thermal recycling.[3] Each method has drawbacks, including excessive energy requirements and the poor quality of recycled products. This renders PET recycling economically uncompetitive with the production of "virgin" PET materials from fresh feedstocks of EG and TPA, which are generally derived from petrochemicals.[4]

Biocatalytic hydrolysis of PET is emerging as a viable route for PET recycling.[5] The first unambiguous description of a "PETase" capable of catalyzing the hydrolysis of PET was reported in 2005, when Müller et al. isolated a cutinase (*Tf*H) from *Thermobifida fusca* DSM43793 that depolymerized PET films by 54% after 21 days of incubation at 55 °C.[6] Another important development was the isolation and characterization of a cutinase (HiC) from the thermophilic fungus *Humilica insolens* that was maximally active at 70–80 °C and could achieve nearly quantitative degradation of amorphous PET films after 96 h at similarly elevated temperatures.[7] In 2012, Kanaya et al. identified a thermostable cutinase (LCC-PETase) that was produced by an unidentified prokaryote from leaf compost and belonged to the α/β hydrolase fold-5 subgroup (IPR029059) of the α/β hydrolase superfamily.[5] This discovery was followed by Yoshida et al., who isolated and characterized a mesophilic PETase and MHETase (dubbed *Is*PETase and *Is*MHETase, respectively) that enabled *Ideonella sakaiensis* to metabolize and grow on PET wastes.[8] *Is*PETase-catalyzed hydrolysis of PET was found to produce mono(2-hydroxyethyl) terephthalate (MHET) as the major product, while *Is*MHETase was shown to convert MHET to TPA and EG. Both enzymes belong to the α/β-hydrolase superfamily and share the conserved catalytic triad of His-Asp-Ser residues that typify this class of enzyme.[9] It has been proposed that differences in the "lid domains" of *Is*PETase and *Is*MHETase are responsible for the substrate specificities of these enzymes.[9]

Recent studies have focused on improving the thermostability and efficiency of PETases to make them useful against real-world PET waste at industrial scales. As the glass transition

Z. Hu, D. L. Zechel, G. Howe
Department of Chemistry
Queen's University
Kingston, ON, Canada
E-mail: graeme.howe@queensu.ca
K. Klupt, Z. Jia
Department of Biomedical and Molecular Sciences
Queen's University
Kingston, ON, Canada

Supporting information for this article is available on the WWW under https://doi.org/10.1002/cbic.202500065

temperature (T_g) of dry PET is 70–80 °C,[10] PETases that function at similarly elevated temperatures are desirable, since at these temperatures, individual strands of PET are thought to be more accessible to enzyme active sites. Even when considering the water-induced crystallization effects that reduce the effective T_g of PET[11] (recent studies place the surface glass transition temperature of PET in water at $T_g = 40–45$ °C[12]), increasingly stable PETases are desirable to prolong the useful lifetime of the biocatalyst. Directed evolution and genome mining studies have identified variant PETases with enhanced thermostabilities and catalytic efficiencies, including LCC^{ICCG}[13] LCC^{WCCG},[13] PHL7,[14] HOT-PETase,[15] and Fast-PETase.[16] Remarkably, one such engineered PETase can break down 90% of 20 kg of PET waste (pretreated with extrusion and micronization) in less than three days.[8,17]

Although early adopters are now implementing enzymatic PET recycling systems on industrial scales,[18] significant questions about the nature and evolution of these enzymes remain. We were interested in assessing how widespread PET-active enzymes are within the α/β hydrolase superfamily. Recent works have also investigated the diversity of sequences that enable enzymatic PET depolymerization,[19] with one study employing bioinformatics and machine learning to identify more than 70 putative thermotolerant PETases comprising seven distinct phylogenetic groups.[20] While most of the 38 sequences confirmed to be active against PET were annotated as carboxylic ester hydrolases (EC3.1.1.-) or cutinases (EC3.1.1.74), more distantly related proteins (i.e., peptidases (EC3.1.1.74)) were also among those confirmed to be active against PET. Recent bioprospecting efforts by Fan et al.[21] have also demonstrated the diversity of sequences that are active against PET by mining the ≈2.5 million unique sequences in their Global Ocean Microbiome Protein Catalogue for proteins with homology to *Is*PETase. Nearly 1,600 such proteins were identified within this collection that could be grouped into seven distinct clades with no dependence on the geographic location of sampling sites. Six proteins were prioritized for in vitro characterization based on their association with extremophiles or extreme ecological niches, and three of these proteins catalyzed PET hydrolysis, suggesting that a significant proportion of the 1,600 putative PETases are authentic PET-degrading enzymes. Intriguingly, the activities of the novel PETases mined from the genomes of the ocean microbiome were enhanced by high salt concentrations, likely reflecting the halophilic nature of the corresponding host marine microbes.

Given the importance of thermostability for efficient PET processing, we used targeted genome mining to search for novel PET-active α/β hydrolases from thermophilic microorganisms. As mutations introduced through directed evolution to enhance activity are often accompanied by compensatory decreases in stability of the protein,[22] we envisioned that the identification of novel, naturally stable PETases would enable more extensive explorations of sequence space while still retaining sufficient stability for industrial purposes. To complement the previously described search for *Is*PETase homologs,[21] we used LCC-PETase as the seed sequence to construct sequence similarity networks (SSNs) and identified ten genes from thermophiles that encoded putative PETases. This work presents structural and biochemical analysis of these novel enzymes against PET and structurally related substrates. Each evaluated protein exhibited significant thermostability, potentially making them useful starting points for directed evolution campaigns aiming to produce new PETases that are both stable and catalytically efficient. Finally, the apparent "hit rate" for PETases within the α/β hydrolase fold-5 subfamily highlights the underappreciated prominence of PET-degrading activity in Nature and the effectiveness of genome mining for finding new PETases.

2. Results and Discussion

2.1. Genome Mining for Thermostable PETases Using Sequence Similarity Networks

The LCC-PETase[17] (accession ID: G9BY57) was used as the seed sequence for constructing a PETase SSN. First, the InterProScan webtool[23] was used to verify that LCC-PETase is a member of IPR029059 (α/β-hydrolase fold-5 subfamily). At an alignment score of 45 (corresponding to a %ID cut-off of ≈26%), LCC-PETase was partitioned into a small cluster of ≈80 unannotated genes (**Figure 1**, forest green), none of which were from thermophiles. In contrast, the largest cluster (Figure 1, red) contained several candidate genes encoding putative thermophilic enzymes. Genes were initially prioritized based on 1) conservation of the LCC-PETase catalytic triad (Ser165, Asp210, His242; LCC-PETase numbering) and 2) the reported growth temperature of the host organisms. AlphaFold2[24] was then used to generate structural predictions for proteins of interest, and each prediction was aligned with the experimentally derived structure of LCC-PETase (PDB ID: 6THS) using the MatchMaker function of ChimeraX.[25] As expected for members of the α/β-hydrolase fold-5 subfamily, the overall folds of predicted structures exhibited very low global root mean square deviation (RMSD) when superimposed with LCC-PETase (Table S1, Supporting Information). These structural alignments were also used to

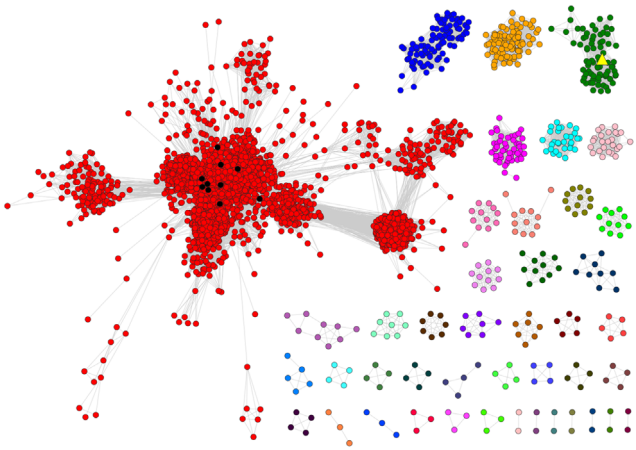

Figure 1. SSN for the α/β hydrolase fold-5 subfamily (IPR029059) constructed at an alignment score of 45 (%ID cutoff ≈26%). The proteins studied in this work (●) were contained in the large, red cluster, whereas LCC-PETase (△) was found in the smaller, forest green cluster.

Table 1. Database identifiers and source organisms for proteins discussed in this work. Maximum reported growth temperatures of these organisms are presented alongside the melting temperature (T_m) and the percent identity matrix illustrating the interrelatedness of each protein.

Protein	Database Identifier	Source Organism	Growth Temperature (°C)[a]	T_m (°C)[b]	Percent ID matrix[c]									
LCC-PETase	G9BY57	Unknown prokaryote	N/A	85	100									
TrmA	E8N6D9	*Anaerolinea thermophila*	60	79	22	100								
BelC	A0A0P6XYT2	*Bellilinea caldifistulae*	65	65	21	53	100							
OcnT	A0AA45C7N1	*Oceanotoga teriensis*	70	74	18	46	47	100						
AroC	I0I495	*Caldilinea aerophila*	65	85	20	55	52	40	100					
TrmN	HEM55323.1	*Thermodesulfobium narugense*	65	69	20	48	43	47	48	100				
TrmD	A0A0P6Y522	*Thermanaerothrix daxensis*	73	79	22	59	56	43	53	44	100			
TrmH	A0A326UD21	*Thermosporothrix hazakensis*	58	57	18	40	36	39	43	43	40	100		
TrmO	B8CYE8	*Halothermothrix orenii*	70	nd[d]	20	47	46	48	45	48	43	40	100	
AroL	A0A540VCZ8	*Litorilinea aerophila*	65	nd[d]	20	49	49	39	55	40	51	39	42	100
NaTrm	B2A7I3	*Natranaerobius thermophilus*	56	nd[d]	20	48	41	40	38	39	40	32	45	41	100

[a]Maximum reported growth temperatures taken from references.[48] [b]T_m values determined by variable temperature CD spectroscopy (see Section 4, Methods and Materials). [c]Values obtained using the Clustal Omega multiple sequence alignment webtool. [d]nd = not determined.

evaluate the predicted active site architecture in proteins of interest. In each of the ten enzymes selected for experimental characterization (**Table 1**), the residues comprising the putative catalytic triad were found to be essentially coincident with the corresponding residues in LCC-PETase (Figure S1 and S2, Supporting Information). The ten enzymes exhibit 18–22%ID with LCC-PETase, and 30–60%ID with one another (Table 1, Figure S1, Supporting Information), thus providing a diverse sequence space to explore for thermostable PETases.

2.2. Esterase Activity with an Activated Substrate

Each PETase was overexpressed in *E. coli* with N-terminal His_6 tags and purified by immobilized metal affinity chromatography (IMAC) (Figure S3, Supporting Information). Repeated attempts to overexpress and purify TrmO, AroL, and NaTrm were unsuccessful, and since TrmN could only be partially purified by IMAC, kinetic comparisons with that protein should be interpreted with caution. The purified enzymes were first tested for their capacity to hydrolyze esters with *p*-nitrophenyl butyrate (*p*NPB) as a substrate.[26] Since most characterized PETases (including both *Is*PETase and LCC-PETase) have been shown to be maximally active at slightly alkaline conditions,[18,27] each purified enzyme was tested for hydrolytic activity against *p*NPB at pH values of 8 and 9 (50 mM Tris–HCl, 30 °C). All tested enzymes catalyzed the hydrolysis of *p*NPB and exhibited standard Michaelis–Menten behavior, except for BelC, which could not be saturated with substrate (Figure S4, Supporting Information). Likewise, with the exception of BelC, the catalytic efficiencies (k_{cat}/K_M) of each enzyme at pH 8 and 9 were similar (**Table 2**). BelC is a significantly more efficient catalyst for the hydrolysis of *p*NPB at pH 8 ($k_{cat}/K_M = 5100\ M^{-1}\ s^{-1}$), although this appears to be derived from a lower K_M value ($K_M = 70\ \mu M$). While this could be interpreted as an increased affinity for the substrate, the lower K_M value may also arise from an accumulation of the acyl-enzyme intermediate due to rate-limiting deacylation.[28]

2.3. Evaluation of Protein Thermostabilities

Melting temperatures (T_m) of the purified enzymes were measured using variable temperature circular dichroism spectroscopy.[29] Gratifyingly, each protein tested was at least moderately thermostable, with T_m values ranging from 57 to 85 °C (Table 1, Figure S5, Supporting Information). Notably, several proteins (i.e., TrmA, OcnT, AroC, TrmN, and TrmD) exhibited thermostability in excess of the reported growth temperature of the source bacterium. For instance, although AroC was sourced from an organism with a maximal reported growth temperature of 65 °C, the T_m value for purified AroC was significantly higher ($T_m = 85$ °C).

Having established the T_m values and esterase activity of the enzymes, we next examined the stabilities of these proteins over time. Given that PET has a $T_g \approx 70$ °C, PET-degrading enzymes that

Table 2. Michaelis–Menten kinetic parameters for the enzyme-catalyzed hydrolysis of *p*NPB at pH 8 and pH 9. All data were collected at 30 °C.

Protein	pH = 8			pH = 9		
	k_{cat} [s^{-1}]	K_M [mM]	k_{cat}/K_M [$\times 10^2$ M s^{-1}]	k_{cat} [s^{-1}]	K_M [mM]	k_{cat}/K_M [$\times 10^2$ M s^{-1}]
AroC	0.22 (0.01)	0.46 (0.08)	4.8 (0.9)	0.26 (0.06)	0.4 (0.1)	6 (2)
OcnT	0.92 (0.08)	0.9 (0.2)	10 (2)	1.4 (0.2)	1.2 (0.2)	12 (2)
TrmA	0.29 (0.02)	1.4 (0.3)	2.1 (0.5)	0.47 (0.03)	1.2 (0.1)	3.9 (0.4)
TrmD	0.11 (0.01)	0.49 (0.08)	2.2 (0.4)	0.5 (0.1)	2.0 (0.6)	2.4 (0.9)
TrmH	0.25 (0.04)	1.3 (0.3)	1.9 (0.5)	0.34 (0.07)	1.2 (0.3)	2.8 (0.9)
TrmN	0.20 (0.05)	0.5 (0.1)	4 (1)	0.53 (0.08)	1.3 (0.2)	4.1 (0.9)
BelC	0.36 (0.04)	0.07 (0.01)	51 (9)	nd[a)]	nd[a)]	12 (1)[b)]

[a)]nd = not determined. [b)]Value obtained from the slope of a plot of initial rates collected at low [*p*NPB].

remain stable and active at similarly elevated temperatures would likely be ideal for biocatalytic PET recycling.[18] Therefore, we incubated each enzyme at temperatures between 70 and 100 °C, while removing aliquots at various time points to measure residual hydrolytic activity against *p*NPB at 30 °C. Gratifyingly, all of the enzymes retained at least 70% of their initial activity over 24 h at 70 °C (**Figure 2**). Remarkably, several of the enzymes exhibited even greater thermostabilities. While AroC and BelC lost 25% and 40% activity, respectively, following 24 h at 80 °C, OcnT, TrmA, and TrmH lost only ≈10% activity under the same conditions (Figure 2B–D), while TrmD showed no significant loss of activity (Figure 2F). Likewise, while 24 h at 90 °C caused TrmA to lose half of its initial activity (Figure 2B), OcnT retained nearly 100% of the initial activity, while AroC and TrmH retained ≈90% of the initial activity. Finally, we examined the impact of boiling the enzymes for one hour. While TrmD lost about 80% of the initial activity after this treatment, TrmA and TrmH lost only ≈20% and ≈25% activity, respectively. Remarkably, OcnT retained 100% activity after one hour at 100 °C. Interestingly, these results show that high T_m values do not necessarily correspond to the active lifetime of an enzyme at a given temperature. For example, the T_m value of OcnT (T_m = 74 °C) is lower than that of both TrmA and TrmD (T_m = 79 °C), and yet OcnT is active at elevated temperatures for longer periods than either TrmA or TrmD (Figure 2). Notably, a recent study also described several PETases that appeared to remain stable and active at temperatures exceeding the melting temperatures of these proteins.[30]

2.4. Characterization of PETase Activity

We next examined the hydrolytic activity of the enzymes against a closer structural mimic of PET. We synthesized 3PET

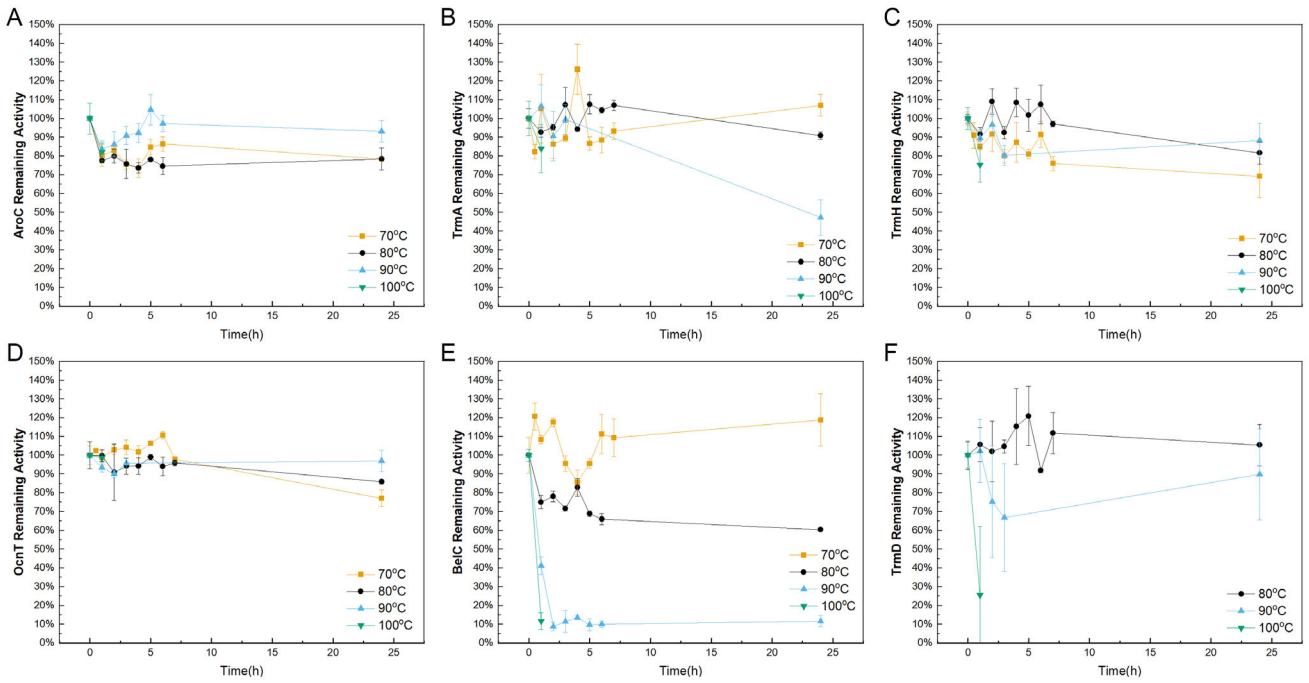

Figure 2. Residual hydrolytic activities against *p*NPB were measured as a function of the length of incubation at various temperatures (70 °C (yellow), 80 °C (black), 90 °C (blue), or 100 °C (green)). A) AroC, B) TrmA, C) TrmH, D) OcnT, E) BelC, and F) TrmD were incubated at a given temperature for the indicated time before residual activities were measured at pH 8.0 (50 mM Tris–HCl), 30 °C.

(bis(benzoyloxyethyl) terephthalate) to serve as a mimic of a trimer of PET (Scheme S1, Supporting Information).[31] Although 3PET is sparingly water-soluble, aqueous emulsions of this compound can be produced, and the decrease in turbidity as 3PET is converted to the water-soluble benzoic acid, TPA, and EG can provide a simple assay of PETase activity.[32] Initial rates were obtained by recording OD_{600} values over time following addition of the enzyme. Six of the purified enzymes were tested against 3PET at pH 8 (50 mM Tris-HCl) and 45 °C, and each was found to catalyze a reduction in turbidity over 16 h. BelC and OcnT gave the highest initial rates of clearance in the first hour (**Table 3**), consistent with the relative catalytic efficiencies observed with *p*NPB as substrate (Table 2). While k_{cat}/K_M values obtained with *p*NPB suggested that BelC and OcnT were the most efficient hydrolases, the agreement between the trends in activities obtained with 3PET and *p*NPB is generally poor, likely reflecting the significant structural differences of these substrates.

Having observed enzyme-catalyzed clearance of the 3PET emulsions, we next assayed both the benchmark PETase LCC^{ICCG} and the putative PETases against authentic PET plastics. First, PET nanoparticles were made into an aqueous emulsion with hexafluoroisopropanol.[33] Each enzyme was added to the solution and the mixture was incubated at 65 °C for one hour. The amount of TPA released from the PET emulsion was quantified using a previously established assay[34] that employs Fenton chemistry to convert TPA into the fluorescent 2-hydroxyterephthlate (**Table 4**). The novel enzymes evaluated here produced variable quantities of TPA, with OcnT, TrmA, and TrmH being the most effective, while AroC and TrmD did not catalyze the release of statistically significant quantities of TPA. While the results in Table 4 demonstrate that a subset of the novel PETases identified here catalyze the release of TPA from emulsified PET, these enzymes are considerably less efficient catalysts for this process than LCC^{ICCG}. As LCC^{ICCG} is an engineered PETase, it is not particularly surprising that the naturally occurring proteins described are less efficient PETases.

A comparison of the results in Table 3 and 4 also suggests interesting differences in the apparent specificities of the novel enzymes toward 3PET and emulsified PET nanoparticles. Most notably, the clearance assay with 3PET indicates BelC and OcnT are the most efficient enzymes (Table 3), whereas the Fenton-based assays that specifically detect TPA suggest that BelC is minimally active and OcnT is a relatively efficient catalyst (Table 4). This result would be consistent with MHET being the major product of the BelC-catalyzed degradation of PET, as the Fenton-based assay will only detect TPA released from the polymer. In contrast, results presented in Table 4 suggest that TPA is the major product of the OcnT-catalyzed PET hydrolysis.

Table 3. Initial rates of clearance of an aqueous emulsion of 3PET. All data were collected at pH 8.0 (50 mM Tris-HCl), 45 °C. Standard deviations derived from triplicate measurements are provided in brackets.

Protein	AroC	OcnT	TrmA	TrmD	TrmN	BelC
$\mu mol_{3PET}/(mg_{Enzyme}*h) \times 10^4$	19.0 (0.3)	44.0 (0.4)	12.0 (0.2)	5.20 (0.08)	9.0 (0.1)	42.0 (0.4)

Table 4. Quantification of TPA released from an aqueous PET emulsion. Reactions were done at pH 8.0 (50 mM Tris-HCl), 65 °C. Standard deviations derived from triplicate measurements are provided in brackets.

Protein	AroC	OcnT	TrmA	TrmD	TrmH	TrmN	BelC	ICCG
$\mu mol_{TPA}/(mg_{enzyme}*h) \times 10^2$	2.4 (2.4)	11 (1)	4.8 (1.2)	0.2 (0.4)	3.6 (0.2)	1.0 (0.1)	0.2 (0.1)	45 (4)

These results mirror previous observations that different PETases will produce different distributions of MHET, TPA, and EG during the catalyzed degradation of PET.[35]

2.5. Characterization of PETases against PET Film

As useful PETases will need to be active on real-world postconsumer PET, the enzymes were next evaluated for their ability to degrade PET films. Each enzyme (final concentration 1 nM) was incubated with amorphous PET film (Goodfellow) for seven days at 65 °C and pH 8 (50 mM Tris–HCl). Every 24 h, an aliquot was removed and analyzed by ultra-performance liquid chromatography-mass spectrometry (UPLC-MS). This same analysis was also conducted using LCC^{ICCG}, although the assay with this protein was conducted over two days, due to the superior performance of this catalyst. Of the novel proteins characterized here, only BelC, OcnT, and TrmN were found to be active against PET film, whereas no products of PET hydrolysis were detected with the remaining enzymes. Over the course of this incubation, these three enzymes clearly catalyzed the formation of varying levels of TPA, MHET, and bis(2-hydroxyethyl) terephthalate (BHET) (**Figure 3**). BelC and TrmN were found to release MHET as the major product during the initial portions of the assay, with TPA gradually accumulating over the course of the week (Figure 3A,B). This "burst" of MHET production was also observed with LCC^{ICCG}, consistent with previous examinations of the product profile associated with this benchmark PETase (Figure S10, Supporting Information). Intriguingly, the product profile associated with the OcnT-catalyzed depolymerization of PET film suggested that this enzyme releases TPA as the major product over the course of the assay (Figure 3C). Each of these enzymes was also found to produce low and relatively constant concentrations of BHET. The observation that BelC produces MHET almost exclusively early in the reaction with PET film, while OcnT produces TPA as the major product, is consistent with results obtained with the TPA-specific activity assay against emulsified PET nanoparticles (Table 4).

The residual activity of BelC, TrmN, and OcnT was also assayed during the PET film degradation study, whereby an aliquot of the reaction mixture was removed at the beginning and end of the one-week assay. The residual hydrolytic activity of each enzyme was then assayed against *p*NPB (Figure 3). These enzymes were found to exhibit widely variable levels of residual activity following the one-week assay at 65 °C, with BelC, TrmN, and OcnT retaining ≈25%, 50%, and 90% activities, respectively. Of the three enzymes active against PET film, BelC exhibited the lowest T_m but was also the most efficient enzyme against both *p*NPB and 3PET. BelC was also the most efficient of these enzymes against PET film, releasing ≈80 μM of TPA and ≈25 μM of MHET over

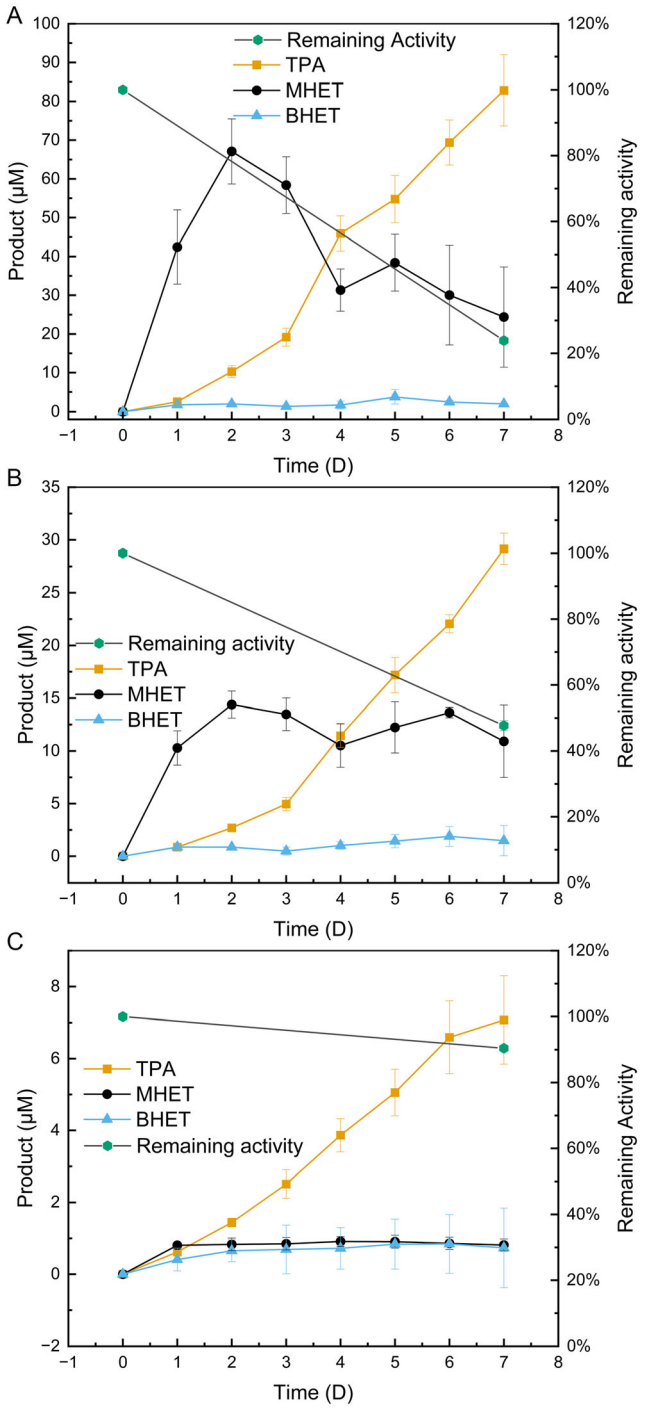

Figure 3. Evaluating hydrolytic activity against PET film. Product distributions obtained with A) BelC, B) TrmN, and C) OcnT are shown over the course of one week of reaction with PET film at 65 °C, pH 8. Data points are as follows: TPA (yellow square), MHET (black sphere), BHET (blue triangle), residual enzyme activity toward pNPB (green sphere).

the course of the week-long assay (Figure 3A). The high efficiency that BelC exhibited on *p*NPB, 3PET emulsions, and PET films may provide some confidence that small molecule mimics of PET can serve as useful compounds to enable comparative kinetic analyses of PETases. In contrast, OcnT is more stable than BelC, and correspondingly, OcnT catalyzed the release of only ≈8 μM of TPA and a miniscule amount of MHET under identical conditions (Figure 3C).

The quantity of degradants released from the PET film was then used to determine the extent of depolymerization of the substrate by LCC^{ICCG} and the three novel enzymes found to be active against films. Although BelC, TrmN, and OcnT are unambiguously active against PET film, the week-long treatment with each enzyme resulted in only 1.2% ± 0.2%, 0.44% ± 0.03%, and 0.08% ± 0.01% depolymerization, respectively. While these enzymes might serve as useful seed sequences for directed evolution campaigns to generate PETases with altered properties, each protein is significantly less efficient at depolymerization than engineered LCC^{ICCG}. In fact, LCC^{ICCG} was shown to achieve nearly quantitative depolymerization of postconsumer PET waste after only 24 h under similar conditions.[13] A more direct comparison was facilitated by incubating LCC^{ICCG} with amorphous PET film at 65 °C and pH 8 (50 mM Tris-HCl) for two days. After this shortened assay, LCC^{ICCG} had depolymerized 32% ± 3% of the film substrate, demonstrating the substantial difference in efficiencies separating BelC, TrmN, and OcnT from this engineered PETase.

Since AroC, TrmA, TrmD, and TrmH were apparently unable to hydrolyze PET film, the level of residual activity of each protein was assayed against *p*NPB following the week-long incubation. While TrmD was largely inactive following the incubation with the film, the three remaining proteins retained significant levels of hydrolytic activity the 7-day reaction at 65 °C (Figure S9, Supporting Information). The lack of reactivity toward PET film by these enzymes may reflect differences in substrate specificity as well as access to the PET polymer chain. Both the PET emulsion assay and PET film assays were conducted at a temperature below the T_g of PET. At this temperature, the emulsified PET nanoparticles would likely be more accessible to the enzymes than the PET film. In this context, it is notable that the Auclair lab has recently demonstrated that the commercial cutinase HiC is able to hydrolyze highly crystalline PET under moist-solid conditions.[36]

2.6. Structural Characterization of AroC

We also attempted to structurally characterize several of the proteins described here to better understand their activities and thermostabilities. While all proteins were subjected to crystallization screening, conditions could only be identified for the growth of high-quality AroC crystals. This protein is not active on PET film and is minimally active on PET nanoparticles (Table 4), but the enzyme does exhibit a remarkably high T_m (85 °C, Table 1) and catalyzes the hydrolysis of 3PET (Table 3). As such, structural characterization of AroC was pursued to gain insight into the thermostability of this protein and, potentially, the stabilities of the other hydrolases were described here. Additionally, the experimentally determined structure of AroC could be compared with the predicted structure of this protein to ensure that AlphaFold2 can accurately predict the structures of the α/β hydrolase fold-5 subfamily members that could not be crystallized.

The structure of AroC was resolved to a resolution of 2.25 Å (PDB: 9EH6) (**Figure 4**). The enzyme crystallized as a homodimer, with each monomer exhibiting the canonical α/β hydrolase

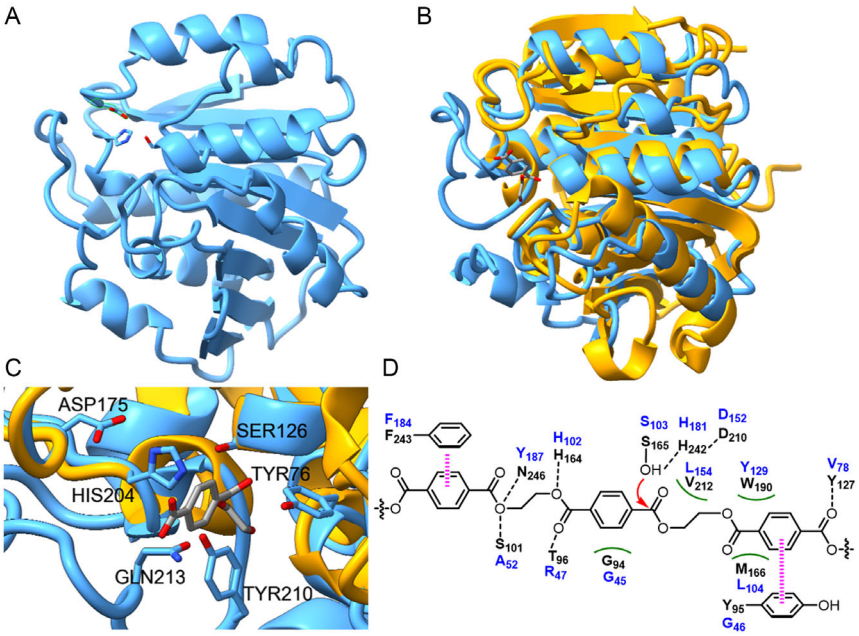

Figure 4. A) The X-ray crystal structure of AroC (PDB: 9EH6) with catalytic triad shown as sticks. B) Alignment of AroC (blue) with LCC-PETase (PDB: 7VVE, yellow) bound to MHET (gray sticks). C) Alignment of AroC and LCC-PETase active sites. MHET is shown in gray, AroC residues in blue sticks. D) Schematic of LCC-PETase active site residues predicted to interact with a trimeric oligomer of PET.[13] LCC-PETase residues shown in black, corresponding AroC residues given in blue. Hydrogen bonds, hydrophobic contacts, and aromatic interactions are shown as black dashed bonds, green curves, and magenta hashed bonds, respectively.

fold made up of eight β-strands arranged into a central mixed β-sheet that is flanked by six α-helices (Figure 4A).[37] AroC has an additional N-terminal α-helix (residues A_{30}QALASL$_{36}$) that serves as a seventh flanking α-helix (Figure S1, Supporting Information). The AroC structure was then compared to the X-ray crystal structure of a mutant LCC-PETase in which the catalytic serine was mutated to an alanine (PDB: 7VVE). The structures exhibited an RMSD of 1.11 Å between 93 pruned atom pairs (8.16 Å across all 193 pairs; Figure 4B) and the catalytic triad residues were effectively coincident (Figure S2A, Supporting Information). However, AroC has a distinctive loop (residues G_{208}WYGEQPGDNPATIS$_{222}$) that folds over the active site (Figure 4B) that is not shared with LCC-PETase (Figure S1, Supporting Information).

AlphaFold2 was then used to predict the structure of AroC, and this prediction was compared to the X-ray crystal structure. The alignment of the two structures exhibited a global RMSD of only 0.672 Å, suggesting that AlphaFold2 accurately predicts the structures of α/β hydrolase fold-5 subfamily. As such, the structures of the nine other proteins described in this work were predicted and aligned with the experimentally derived structure of AroC. This comparison indicated that each protein harbors the distinctive loop (G_{208}–S_{222}; AroC numbering) that is absent in LCC-PETase, and a multiple sequence alignment demonstrated significant sequence conservation within and immediately preceding this loop: F_{207}GxY(G/E)xQx(G/E)Dxxxxl(S/T)$_{222}$ (AroC numbering, Figure S11, Supporting Information). While this conservation is intriguing, the role of this loop is not entirely clear: of the 13 first shell active site residues that LCC-PETase is predicted to use to interact with a model of a PET trimer,[13] AroC shares 4 identical residues, and 6 others that are similar in polarity and size (Figure 4C,D, Figure S1, Supporting Information). F207 of AroC is predicted to make a conserved π-interaction with a terephthalate group, whereas Y210 and H125 are predicted to replicate H-bonds to ester linkages, and G68, L177, Y152, and L127 are homologs to residues in LCC-PETase that form hydrophobic contacts with the substrate (Figure 4D).

Next, the predicted structures of BelC, OcnT, TrmA, TrmD, TrmH, TrmN, along with the X-ray crystal structure of AroC, were used to rationalize the thermostability of the enzymes. The number of salt bridges present on the surface of each protein was determined and compared to the T_m value for each protein (**Figure 5**). In general, the T_m of the enzyme correlates well with

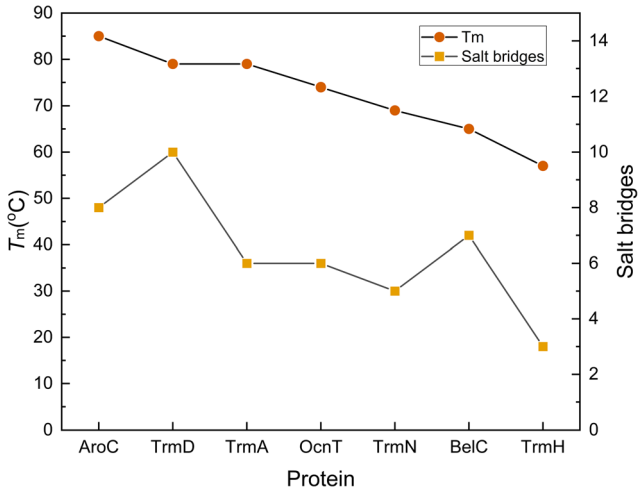

Figure 5. Correlation between PETase T_m values and the number of surface salt bridges. The number of salt bridges was determined from the X-ray crystal structure of AroC, and AlphaFold2 structures for the remaining enzymes.

the number of surface salt bridges on the exterior of the protein, with TrmD and BelC having T_m values higher than expected. This is consistent with the finding that salt bridges are more abundant in hyper-thermostable proteins.[38] At higher temperatures, the energetic penalty associated with desolvation of charged residues decreases significantly, such that salt bridges are largely stabilizing at elevated temperatures.[33] While the observed correlation between thermostability and the number of salt bridges is not exact, it does implicate these ionic interactions as being at least partially responsible for imbuing the enzymes described here with exceptional thermostabilities.

3. Conclusion

In this study, we made use of SSNs to mine the α/β hydrolase family for novel PET-degrading enzymes from thermophilic organisms. This approach proved to be highly efficient: out of ten genes encoding putative thermophilic PETases from α/β hydrolase_5 subfamily, seven soluble proteins were purified and shown to be active toward a trimeric mimic of PET and PET nanoparticles, and three of these enzymes were also capable of degrading PET film. Given that these proteins were quite dissimilar to LCC-PETase (%ID = 18–22%), results presented here also suggest that PET-active proteins may be more widely distributed across the α/β hydrolase family than previously appreciated. Each new PETase described here also exhibited high thermostabilities, and structural analysis demonstrated a correlation between the number of surface salt-bridges with observed T_m values. With advancements in the understanding of PETase mechanisms, these naturally thermostable PETase variants can serve as scaffolds for directed evolution to engineer variants that are both thermostable and catalytically efficient. Overall, this work not only expands our knowledge in enzymatic PET degradation but also provides a template for the discovery of extremozymes for other applications.

4. Experimental Section

General

Chemicals used to make media and buffers were obtained from Bioshop. Genes encoding PETases were synthesized into expression vectors by BioBasic (Canada). In cases where SignalP 6.0 predicted signal peptides, the corresponding portion of the gene was removed.[39] The genes were codon optimized for expression in *E. coli* and cloned into the NdeI and XhoI sites of pET-26b (+) to encode each enzyme with an C-terminal His_6-tag. Optimized gene sequences are given in the Supplementary Information (Table S4, Supporting Information). Unless otherwise stated, all cultivation media for *E. coli* was supplemented with 50 μg mL^{-1} kanamycin. Plysurf A210G surfactant was obtained from Dr. Sofia Lemak and Prof. Alexander F. Yakunin (University of Toronto). PET film was purchased from GoodFellow, PET nanoparticles were purchased from Nanochemazone, and Ni^{2+} Sepharose high-performance resin was purchased from Cytiva. *E. coli* BL21(DE3) and LOBSTR cells were obtained from New England Biosciences and Fisher Scientific, respectively.

SSN Analysis

LCC-PETase (accession ID: G9BY57) was analyzed by the InterProScan webtool to assign this enzyme to the IPR029059 (α/β-hydrolase fold-5) family. The Enzyme Function Initiative's Enzyme Similarity Tool (EFI-EST)[40] was then used to conduct an all-by-all BLAST for all members of this protein family. An alignment score of 45 was used to visualize the resulting network in Cytoscape 3.9.1. Sequences contained in this network that were from thermophiles were identified using Cytoscape's ability to filter nodes on the basis of the name of the host organism.

Protein Expression and Purification

Plasmids encoding PETases were transformed into chemically competent *E. coli* cells by heat shock and plated onto lysogeny broth (LB)-agar supplemented with 50 μg mL^{-1} kanamycin. AroC, TrmA, and OcnT were expressed in *E. coli* BL21(DE3) cells, while TrmD, TrmN, BelC, and TrmH were expressed in *E. coli* LOBSTR cells. Following overnight growth, a single colony was picked and used to inoculate 10 mL of sterile LB media. The next day, this overnight culture was used to inoculate 1 L of LB. The culture was allowed to grow at 37 °C and 180 rpm until an OD_{600} of 0.6–0.8 was reached. After incubating the cells on ice for 10 min, expression was then induced by the addition of isopropyl β-D-1-thiogalactopyranoside to a final concentration of 0.5 mM. The culture was then shaken at 37 °C and 180 rpm for an additional 3 h before the cells were harvested by centrifugation at 4 °C and 4000 × *g* for 10 min. Harvested cells were resuspended in binding buffer (20 mM Tris–HCl, pH 7.6, 100 mM NaCl, 20 mM imidazole, 10% glycerol v/v) and lysed by three passes through an EmulsiFlex C-5 homogenizer (Avestin, Ottawa) at 10,000–15,000 psi. Cellular debris was then removed by centrifugation at 16,000 × *g* for 1 hr and the supernatant was loaded onto a Ni^{2+}-NTA resin that had been preequilibrated with binding buffer. The column was then washed with 10–15 column volumes (CVs) of binding buffer followed by elution of the protein of interest with 3–5 CVs of elution buffer (20 mM Tris–HCl, pH 7.6, 100 mM NaCl, 500 mM imidazole, 10% glycerol v/v). Fractions containing pure enzyme were determined by SDS-PAGE, pooled and concentrated using a 10 kDa MWCO centrifugal filter unit. Concentrated samples were buffer exchanged into storage buffer (40 mM Tris–HCl, pH 7.6, 100 mM NaCl, and 10% glycerol v/v) using a PD-10 desalting column or a 10 kDa MWCO centrifugal filter unit. Protein concentrations were measured by absorbance at 280 nm using extinction coefficients calculated for each protein using the ProtParam tool from Expasy.[41]

Enzyme Activity Assays with *p*NPB

Reactions to assay esterase activity were performed in 976 μL 50 mM Tris-HCl (pH 8 or 9) equilibrated at 30 °C. Aliquots of 20 μL *p*NPB dissolved in acetone were added to achieve the desired final substrate concentrations. The reaction was initiated by the addition of 4 μL concentrated enzyme, and reaction progress was monitored by absorbance at 405 nm using an Agilent Technologies G9864A spectrometer. Spontaneous rates of hydrolysis were measured prior to adding enzyme and subtracted from the observed enzymatic rate. Initial rates were measured at substrate concentrations between ≈0.2× and ≈5× the final K_M values, where possible. Plots of initial rates versus substrate concentration were fit to the Michaelis Menten equation using Origin Lab 2024. Values of k_{cat} were determined using calculated enzyme extinction coefficients for enzyme concentrations and $\varepsilon_{405} = 18{,}000\ M^{-1}\,cm^{-1}$ for *p*-nitrophenolate.[42]

T_m Measurements of Enzymes

Protein samples (300 μL of 1 mg mL^{-1}) were loaded into a quartz cuvette (Hellma USA Inc., round cylindrical cuvette, 1 mm pathlength)

and placed into a Chirascan V100 CD spectroscopy instrument (Applied Photophysics Ltd.). Samples were incrementally heated from 20 to 90 °C in 2.5 °C steps. Ellipticity was measured as a function of temperature between 180 and 260 nm. The melting temperature (T_m) is the temperature at which the fraction unfolded (F_u) and fraction folded (F) are equal. Fraction unfolded is calculated using the equation $F_u = (F_o - F)/(U_f - F)$ where F_o is the ellipticity value at each temperature, F is the ellipticity value at low temperature, and U_f is the ellipticity value at the highest temperature.

Enzyme Thermostability Analysis

Aliquots of enzyme at 100 μM in storage buffer (40 mM Tris–HCl, pH 7.6, 100 mM NaCl, 10% glycerol v/v) were placed in a water bath set at the desired temperature for 0 to 24 h. At a given time, an aliquot of enzyme was removed, centrifuged at 8500 rpm for 1 min, then placed on ice. 4 μL of supernatant was then used to initiate the hydrolysis of 0.5 mM *p*NPB at 30 °C in 1 mL 50 mM Tris–HCl, pH 8. Initial rates were measured in triplicate with three individual aliquots.

3PET Synthesis[43]

3PET was synthesized as described previously (Scheme S1, Supporting Information), and purified by flash silica gel chromatography using toluene: ethyl acetate 5:1 (v/v). NMR spectroscopic analysis of pure 3PET (Figure S6, Supporting Information) matched the literature description.[43]

Enzyme Activity Assay with 3PET

A 3PET emulsion was formed by dissolving 0.1 g of 3PET in 5 mL of acetone and adding 20 mg of the surfactant Plysurf A210G. The mixture was poured into 20 mL of Tris–HCl (50 mM, pH 8) and suspended by sonication at maximum frequency (Fisher Scientific Sonic Dismembrator Model 100) on ice for 30 min. The solution was then stirred at 60 °C for 30 min, followed by stirring at room temperature overnight to be ready for use. The 3PET emulsion was diluted with 50 mM Tris–HCl (pH 8.0) to a final OD_{600} of ≈1. Then, 150 μL of the diluted 3PET emulsion was added to each well of a 96-well plate along with 50 μL of enzyme solution to achieve a final concentration of 15–400 μM. The plate was shaken (180 rpm) at 45 °C for 72 h using a BioTek Synergy H1 plate reader, and OD_{600} was recorded every 10 min. Triplicate measurements of the initial OD_{600} of a 3PET emulsion were recorded before these mixtures were centrifuged at 13,000 rpm for 10 min to collect the 3PET in the emulsion. Residues were then dried in a 60 °C oven for ≈11 h before being weighed. The mass of the collected 3PET was then correlated to the OD_{600} to convert OD_{600} measurements to approximate masses of 3PET.[33]

Enzyme Activity Assay with PET Nanoparticles

The quantitation of TPA released from PET nanoparticles during enzymatic hydrolysis was determined by oxidatively converting TPA to the fluorescent compound 2-hydroxyterephthalate as described previously.[33] PET nanoparticles were dissolved in 1,1,1,3,3,3-hexafluoro-2-propanol (HFIP) and then added dropwise into water while sonicating on ice at maximum frequency (Fisher Scientific Sonic Dismembrator Model 100). HFIP was subsequently removed by rotary evaporation. 10 μL aliquots of the PET emulsion were dispensed into 96-well plates along with 1–10 μL of enzyme solution (to a final concentration of 1 μM) and a sufficient volume of 500 mM sodium phosphate buffer (pH 8) to bring the total volume to 200 μL. The 96-well plate was then placed in a temperature-controlled shaker (Labnet Vortemp 56) for incubation at 65 °C with shaking at 800 rpm for 60 min. Plates were then centrifuged at 2,844 × *g* and 4 °C for 15 min before transferring 150 μL of the supernatant into a black 96-well plate. Prior to measurements, 25 μL of 5 mM EDTA and 25 μL of 5 mM $FeSO_4$ were added to initiate the oxidation of TPA, and the plates were incubated at room temperature for at least 10 min before fluorescence readings were recorded on a BioTek Synergy H1 plate reader ($\lambda_{ex} = 314$ nm, $\lambda_{em} = 421$ nm). A standard curve of fluorescence versus known concentrations of TPA converted to 2-hydroxyterepthlalate through the Fenton reaction was used to quantify the enzymatic TPA product (Figure S7, Supporting Information).

PET Film Assay

Goodfellow PET film (ES30-FM-000145, 0.25 mm thickness, transparent, amorphous) was cut into 2 mg discs of 6 mm diameter with a standard paper hole punch. The PET discs were placed in a microcentrifuge tube containing 50 mM Tris–HCl, pH8 followed by adding enzymes to a final concentration of 1 nM for a total reaction volume of 1 mL. The reaction was incubated in a Labnet Vortem p56 shaker at 65 °C for 7 days at 800 rpm. Aliquots of 27 μL were removed from the reactions each day and mixed with 3 μL DMSO to assist solubilization of the products of hydrolysis. Samples were sonicated for 5 min and then centrifuged at 21,000 × *g* for 10 min. The solutions were then resolved on a Cortecs T3 UPLC reverse phase column (1.6 μm, 2.1 × 100 mm) using a Waters Acquity UPLC-MS H class system. A 10 μL aliquot of the sample was injected and resolved using a gradient of 89:1:10 to 55:35:10 water/acetonitrile/1% formic acid over 11 min with a flow rate of 0.3 mL min^{-1}. The hydrolysis products (TPA, MHET, and BHET) were detected by absorbance at 240 nm and quantified by comparison to standard curves (Figure S8, Supporting Information). The depolymerization percentage of PET was calculated based on the initial mass of the PET film (2 mg) used in the experiment. The mass was divided by the molecular weight of the PET repeating unit (192.18 g mol^{-1}) to determine the theoretical 100% conversion amount in moles. For each enzyme, the total amount of UPLC-detected depolymerized products—terephthalic acid (TPA), mono(2-hydroxyethyl) terephthalate (MHET), and bis(2-hydroxyethyl) terephthalate (BHET)—was summed in moles. This total was then divided by the theoretical 100% conversion amount to obtain the percentage of PET depolymerization.

AroC X-ray Crystallography

Purified AroC was concentrated to 10 mg mL^{-1} in 40 mM Tris-HCl, pH 7.6, 100 mM NaCl. Crystallization conditions were screened using the Index HT screening kit (Hampton Research Corp) and the final protein crystallization condition after refinement for crystal growth was 100 mM sodium acetate at pH 4.5 with 8% PEG3350. Protein crystals were stored in liquid nitrogen and data collection was performed at the Canadian Light Source synchrotron. Data was auto-processed with XDS and scaled to a maximum resolution of 2.25 Å (Table S3, Supporting Information). The AlphaFold2 predicted structure of AroC was utilized for molecular replacement using MOLREP as part of the CCP4 suite.[44] Water molecules were resolved, and refinement was completed using REFMAC.[45] Coot[46] was used for structure verification and manual refinement to fit the structure into the observed electron density map.[47] The final structure was deposited into the Protein Data Bank as 9EH6.

Acknowledgements

The authors are grateful to John Habib, Katherine Withnall for their assistance with protein production and crystallization. The authors are grateful for the assistance of Dr. Laura van Staalduinen for her

guidance with crystal refinement. The authors thank Dr. Sofia Lemak and Prof. Alexander Yakunin for generously providing samples of PlySurf A210G and *E. Coli* LOBSTR cells. The authors are grateful to the Natural Sciences and Engineering Research Council of Canada and Genome Canada for financial support of this research.

Conflict of Interest

The authors declare no conflict of interest.

Data Availability Statement

The data that support the findings of this study are available in the supplementary material of this article.

Keywords: bioinformatics · enzyme catalysis · polyethylene terephthalate biodegradation · sequence similarity networks · thermostable

[1] a) F. Awaja, D. Pavel, *Eur. Polym. J.* **2005**, *41*, 1453; b) L. De Vos, B. Van de Voorde, L. Van Daele, P. Dubruel, S. Van Vlierberghe, *Eur. Polym. J.* **2021**, *161*, 110840.
[2] A. Chamas, H. Moon, J. Zheng, Y. Qiu, T. Tabassum, J. H. Jang, M. Abu-Omar, S. L. Scott, S. Suh, *ACS Sustainable Chem. Eng.* **2020**, *8*, 3494.
[3] E. Barnard, J. J. Rubio Arias, W. Thielemans, *Green Chem.* **2021**, *23*, 3765.
[4] M. Cronshaw, in *Energy in Perspective* (Ed: M. Cronshaw), Springer International Publishing, Cham **2021**, pp. 179–187.
[5] R. Gao, H. Pan, J. Lian, *Enzyme Microb. Technol.* **2021**, *150*, 109868.
[6] R.-J. Müller, H. Schrader, J. Profe, K. Dresler, W.-D. Deckwer, *Macromol. Rapid Commun.* **2005**, *26*, 1400.
[7] Å. M. Ronkvist, W. Xie, W. Lu, R. A. Gross, *Macromolecules* **2009**, *42*, 5128.
[8] S. Yoshida, K. Hiraga, T. Takehana, I. Taniguchi, H. Yamaji, Y. Maeda, K. Toyohara, K. Miyamoto, Y. Kimura, K. Oda, *Science* **2016**, *351*, 1196.
[9] S. Boneta, K. Arafet, V. Moliner, *J. Chem. Inf. Model.* **2021**, *61*, 3041.
[10] P. J. Holdsworth, A. Turner-Jones, *Polymer* **1971**, *12*, 195.
[11] A. B. Desai, G. L. Wilkes, *J. Polym. Sci. Polym. Symp.* **1974**, *46*, 291.
[12] a) E. Akram, Y. Cao, H. Xing, Y. Ding, Y. Luo, R. Wei, Y. Zhang, *Chin. J. Catal.* **2024**, *60*, 284; b) N. A. Tarazona, R. Wei, S. Brott, L. Pfaff, U. T. Bornscheuer, A. Lendlein, R. Machatschek, *Chem Catal.* **2022**, *2*, 3573.
[13] V. Tournier, C. M. Topham, A. Gilles, B. David, C. Folgoas, E. Moya-Leclair, E. Kamionka, M. L. Desrousseaux, H. Texier, S. Gavalda, M. Cot, E. Guemard, M. Dalibey, J. Nomme, G. Cioci, S. Barbe, M. Chateau, I. Andre, S. Duquesne, A. Marty, *Nature* **2020**, *580*, 216.
[14] P. K. Richter, P. Blázquez-Sánchez, Z. Zhao, F. Engelberger, C. Wiebeler, G. Künze, R. Frank, D. Krinke, E. Frezzotti, Y. Lihanova, P. Falkenstein, J. Matysik, W. Zimmermann, N. Sträter, C. Sonnendecker, *Nat. Commun.* **2023**, *14*, 1905.
[15] E. L. Bell, R. Smithson, S. Kilbride, J. Foster, F. J. Hardy, S. Ramachandran, A. A. Tedstone, S. J. Haigh, A. A. Garforth, P. J. R. Day, C. Levy, M. P. Shaver, A. P. Green, *Nat. Catal.* **2022**, *5*, 673.
[16] H. Lu, D. J. Diaz, N. J. Czarnecki, C. Zhu, W. Kim, R. Shroff, D. J. Acosta, B. R. Alexander, H. O. Cole, Y. Zhang, N. A. Lynd, A. D. Ellington, H. S. Alper, *Nature* **2022**, *604*, 662.
[17] S. Sulaiman, S. Yamato, E. Kanaya, J. J. Kim, Y. Koga, K. Takano, S. Kanaya, *Appl. Environ. Microbiol.* **2012**, *78*, 1556.
[18] G. Arnal, J. Anglade, S. Gavalda, V. Tournier, N. Chabot, U. T. Bornscheuer, G. Weber, A. Marty, *ACS Catal.* **2023**, *13*, 13156.
[19] H. Seo, H. Hong, J. Park, S. H. Lee, D. Ki, A. Ryu, H.-Y. Sagong, K.-J. Kim, *Science* **2025**, *387*, eadp5637.
[20] E. Erickson, J. E. Gado, L. Avilán, F. Bratti, R. K. Brizendine, P. A. Cox, R. Gill, R. Graham, D.-J. Kim, G. König, W. E. Michener, S. Poudel, K. J. Ramirez, T. J. Shakespeare, M. Zahn, E. S. Boyd, C. M. Payne, J. L. DuBois, A. R. Pickford, G. T. Beckham, J. E. McGeehan, *Nat. Commun.* **2022**, *13*, 7850.
[21] J. Chen, Y. Jia, Y. Sun, K. Liu, C. Zhou, C. Liu, D. Li, G. Liu, C. Zhang, T. Yang, L. Huang, Y. Zhuang, D. Wang, D. Xu, Q. Zhong, Y. Guo, A. Li, I. Seim, L. Jiang, L. Wang, S. M. Y. Lee, Y. Liu, D. Wang, G. Zhang, S. Liu, X. Wei, Z. Yue, S. Zheng, X. Shen, S. Wang, et al., *Nature* **2024**, *633*, 371.
[22] J. D. Bloom, F. H. Arnold, *Proc. Natl. Acad. Sci. U.S.A.* **2009**, *106*, 9995.
[23] P. Jones, D. Binns, H.-Y. Chang, M. Fraser, W. Li, C. McAnulla, H. McWilliam, J. Maslen, A. Mitchell, G. Nuka, S. Pesseat, A. F. Quinn, A. Sangrador-Vegas, M. Scheremetjew, S.-Y. Yong, R. Lopez, S. Hunter, *Bioinformatics* **2014**, *30*, 1236.
[24] J. Jumper, R. Evans, A. Pritzel, T. Green, M. Figurnov, O. Ronneberger, K. Tunyasuvunakool, R. Bates, A. Žídek, A. Potapenko, A. Bridgland, C. Meyer, S. A. A. Kohl, A. J. Ballard, A. Cowie, B. Romera-Paredes, S. Nikolov, R. Jain, J. Adler, T. Back, S. Petersen, D. Reiman, E. Clancy, M. Zielinski, M. Steinegger, M. Pacholska, T. Berghammer, S. Bodenstein, D. Silver, O. Vinyals, et al., *Nature* **2021**, *596*, 583.
[25] E. C. Meng, T. D. Goddard, E. F. Pettersen, G. S. Couch, Z. J. Pearson, J. H. Morris, T. E. Ferrin, *Protein Sci.* **2023**, *32*, e4792.
[26] a) T. Tsujita, H. Ninomiya, H. Okuda, *J. Lipid Res.* **1989**, *30*, 997; b) A. Distaso Marco, N. Chernikova Tatyana, R. Bargiela, C. Coscolín, P. Stogios, L. Gonzalez-Alfonso Jose, S. Lemak, N. Khusnutdinova Anna, J. Plou Francisco, E. Evdokimova, A. Savchenko, A. Lunev Evgenii, M. Yakimov Michail, V. Golyshina Olga, M. Ferrer, F. Yakunin Alexander, N. Golyshin Peter, *Appl. Environ. Microbiol.* **2023**, *89*, e01704.
[27] a) A. Carniel, V. d. A. Waldow, A. M. d. Castro, *Biotechnol. Adv.* **2021**, *52*, 107811; b) Y. Gao, Y. Zheng, Z. Qi, Y. Pan, Y. Zhou, S. You, R. Su, W. Qi, M. Wang, *J. Chem. Technol. Biotechnol.* **2024**, *99*, 1860.
[28] K. S. Anderson, K. A. Johnson, *Chem. Rev.* **1990**, *90*, 1131.
[29] N. J. Greenfield, *Nat. Protoc.* **2006**, *1*, 2876.
[30] S. H. Lee, M. Kim, H. Seo, H. Hong, J. Park, D. Ki, K.-J. Kim, *ACS Catal.* **2024**, *14*, 4108.
[31] G. Fischer-Colbrie, S. Heumann, S. Liebminger, E. Almansa, A. Cavaco-Paulo, G. M. Guebitz, *Biocatal. Biotransform.* **2004**, *22*, 341.
[32] D. Ribitsch, S. Heumann, E. Trotscha, E. Herrero Acero, K. Greimel, R. Leber, R. Birner-Gruenberger, S. Deller, I. Eiteljoerg, P. Remler, T. Weber, P. Siegert, K. H. Maurer, I. Donelli, G. Freddi, H. Schwab, G. M. Guebitz, *Biotechnol. Progr.* **2011**, *27*, 951.
[33] S. Farah, T. Tsach, A. Bentolila, A. J. Domb, *Talanta* **2014**, *123*, 54.
[34] L. Pfaff, D. Breite, C. P. S. Badenhorst, U. T. Bornscheuer, R. Wei, *Methods Enzymol.* **2021**, *648*, 253.
[35] K. Chen, Y. Hu, X. Dong, Y. Sun, *ACS Catal.* **2021**, *11*, 7358.
[36] S. Kaabel, J. P. D. Therien, C. E. Deschênes, D. Duncan, T. Friščić, K. Auclair, *Proc. Natl. Acad. Sci. U. S. A.* **2021**, *118*, e2026452118.
[37] M. Nardini, B. W. Dijkstra, *Curr. Opin. Struct. Biol.* **1999**, *9*, 732.
[38] S. Kumar, C. J. Tsai, B. Ma, R. Nussinov, *J. Biomol. Struct. Dyn.* **2000**, *17*, 79.
[39] F. Teufel, J. J. Almagro Armenteros, A. R. Johansen, M. H. Gíslason, S. I. Pihl, K. D. Tsirigos, O. Winther, S. Brunak, G. von Heijne, H. Nielsen, *Nat. Biotechnol.* **2022**, *40*, 1023.
[40] J. A. Gerlt, J. T. Bouvier, D. B. Davidson, H. J. Imker, B. Sadkhin, D. R. Slater, K. L. Whalen, *Biochim. Biophys. Acta.* **2015**, *1854*, 1019.
[41] E. Gasteiger, C. Hoogland, A. Gattiker, S. e. Duvaud, M. R. Wilkins, R. D. Appel, A. Bairoch, in *The Proteomics Protocols Handbook* (Ed: J. M. Walker), Humana Press, Totowa, NJ **2005**, pp. 571–607.
[42] Y.-Y. Zhang, Z.-Q. Mei, J.-W. Wu, Z.-X. Wang, *J. Biol. Chem.* **2008**, *283*, 26591.
[43] G. Fischer-Colbrie, S. Heumann, S. Liebminger, E. Almansa, A. Cavaco-Paulo, G. M. Guebitz, *Biocatal. Biotransform.* **2009**, *22*, 341.
[44] A. Vagin, A. Teplyakov, *J. Appl. Crystallogr.* **1997**, *30*, 1022.
[45] G. N. Murshudov, A. A. Vagin, E. J. Dodson, *Acta Crystallogr., Sect. D: Biol. Crystallogr.* **1997**, *53*, 240.
[46] P. Emsley, K. Cowtan, *Acta Crystallogr., Sect. D: Biol. Crystallogr.* **2004**, *60*, 2126.
[47] a) L. Potterton, J. Agirre, C. Ballard, K. Cowtan, E. Dodson, P. R. Evans, H. T. Jenkins, R. Keegan, E. Krissinel, K. Stevenson, A. Lebedev, S. J. McNicholas, R. A. Nicholls, M. Noble, N. S. Pannu, C. Roth, G. Sheldrick, P. Skubak, J. Turkenburg, V. Uski, F. von Delft, D. Waterman, K. Wilson, M. Winn, M. Wojdyr, *Acta Crystallogr., Sect. D: Biol. Crystallogr.* **2018**, *74*, 68; b) W. Kabsch, *Acta Crystallogr., Sect. D: Biol. Crystallogr.* **2010**, *66*, 125.
[48] a) P. Grégoire, M.-L. Fardeau, M. Joseph, S. Guasco, F. Hamaide, S. Biasutti, V. Michotey, P. Bonin, B. Ollivier, *Syst. Appl. Microbiol.* **2011**, *34*, 494; b)

H. S. Jayasinghearachchi, B. Lal, *Int. J. Syst. Evol. Microbiol.* **2011**, *61*, 554; c) V. Kale, S. H. Björnsdóttir, O. H. Friðjonsson, S. K. Petursdottir, S. Omarsdottir, G. O. Hreggviðsson, *Int. J. Syst. Evol. Microbiol.* **2013**, *63*, 1149; d) K. Mavromatis, N. Ivanova, I. Anderson, A. Lykidis, S. D. Hooper, H. Sun, V. Kunin, A. Lapidus, P. Hugenholtz, B. Patel, *PLoS One* **2009**, *4*, e4192; e) N. M. Mesbah, D. B. Hedrick, A. D. Peacock, M. Rohde, J. Wiegel, *Int. J. Syst. Evol. Microbiol.* **2007**, *57*, 2507; f) K. Mori, H. Kim, T. Kakegawa, S. Hanada, *Extremophiles* **2003**, *7*, 283; g) Y. Sekiguchi, T. Yamada, S. Hanada, A. Ohashi, H. Harada, Y. Kamagata, *Int. J. Syst. Evol. Microbiol.* **2003**, *53*, 1843; h) S. Yabe, Y. Aiba, Y. Sakai, M. Hazaka, A. Yokota, *Int. J. Syst. Evol. Microbiol.* **2010**, *60*, 1794; i) T. Yamada, H. Imachi, A. Ohashi, H. Harada, S. Hanada, Y. Kamagata, Y. Sekiguchi, *Int. J. Syst. Evol. Microbiol.* **2007**, *57*, 2299–2306.

Manuscript received: March 10, 2025
Revised manuscript received: March 11, 2025
Version of record online: April 7, 2025